Low Complexity Detection for Spatial Modulation Aided Sparse Code Division Multiple Access

Luping Xiang, *Member, IEEE*, Yusha Liu, *Student Member, IEEE*, Lie-Liang Yang, *Fellow, IEEE*, and Lajos Hanzo, *Fellow, IEEE*

Abstract—Low-complexity detectors are conceived for the spatial modulation-aided sparse code-division multiple-access (SM-SCDMA). Firstly, the approximate message passing (AMP) algorithm is adapted for the detection of SM-SCDMA, which has less than 1% detection complexity of the state-of-the-art message passing-aided (MPA) detection albeit at a bit error ratio (BER) degradation. Therefore, inspired by the benefits of interference cancellation (IC) and the unique characteristics of SM, an enhanced AMP (EAMP) detector is proposed for mitigating BER degradation without increasing the detection complexity. Finally, the classic expectation propagation (EP) is intrinsically amalgamated with our EAMP detector, leading to a novel EAMP-EP detector, which further reduces the detection complexity of the EAMP algorithm. The three detectors are compared both in terms of their coded and uncoded BER, as well as complexity.

Index Terms—Spatial modulation (SM), sparse code-division multiple-access (SCDMA), nonorthogonal multiple access (NOMA) approximate message passing (AMP) detection.

I. INTRODUCTION

Index modulation (IM), which employs the resource index as an additional means of conveying information, is a promising technique of meeting high energy-efficiency requirements. Hence, IM has attracted intensive research interests over the past few years. In the family of different IM schemes, spatial modulation (SM) [1]–[3], which activates different antennas for conveying extra information, is capable of reducing the complexity of conventional multiple-input multiple-output (MIMO) configurations, such as the Vertical Bell Laboratories Layered Space-Time (V-BLAST) code or space-time block code (STBC) by reducing the number of radio frequency (RF) chains. Specifically, by activating a single one or a subset of the available transmit antennas (TAs), a diverse variety of SM schemes has been proposed. These include *space-shift keying (SSK)* [4], which conveys information by solely exploiting the TA indices, the *SM* scheme of [1], where a single TA is activated to transmit a single amplitude-phase modulation (APM) symbol, *quadrature SM (QSM)* [5], which extends the real-valued SM constellation to both the in-phase and quadrature dimensions, and *generalized SM (GSM)* [6], which simultaneously activates a group of TAs to convey multiple

APM symbols, etc. Euclidean distance-based antenna selection for SM was further investigated in [7]. Low-complexity detection of different SM schemes has been proposed in [6], [8]–[11], such as the distance-based ordered detector of [11] and the compressive sensing (CS) aided detector of [9], [10].

The literature of IM conceived for multiuser communications can be categorized into a pair of subclasses, namely IM-aided orthogonal multiple access (IM-OMA) [12], [13], where each user occupies a single resource element in the time/ frequency or code domain, and IM-aided nonorthogonal multiple access (IM-NOMA) [14]–[20], where each of the orthogonal resources is shared by several users. The focus of this paper is on SM combined with code-domain NOMA techniques, in particular, sparse code-division multiple access (SCDMA) [16], where each user employs a unique low density signature (LDS) [21] to spread the signal over either the time or the frequency domain.

As a benefit of taking full advantage of both the spectral resources and of the energy dissipation, SM-NOMA constitutes a promising technique of supporting a high normalised user load [22], including the Internet-of-things (IoT) [23] and massive machine-type communications (mMTC) scenarios [24]–[26].

Unfortunately, the state-of-the-art message passing-aided (MPA) SM-NOMA detector suffers from high detection complexity. Even though low-complexity SM-OMA detectors have been conceived in [13], [32]–[34], they are unsuited for rank-deficient systems. Hence, reduced-complexity SM-NOMA detectors have been investigated in [27], [28]. In [27], the authors proposed a rotational generalized SM-NOMA scheme and conceived a tailored MPA detector for jointly detecting the antenna grouping and the transmitted symbol. Three low-complexity detectors were proposed in [28] for SM-assisted sparse code multiple access (SM-SCMA). While the successive user detector (SUD) and its modified version (MSUD) attained a significant complexity reduction by as much as 90% at the cost of some BER degradation, the tree-search based fixed-complexity sphere decoder (FCSD) achieved a near-MPA BER performance at about only half of the MPA detection complexity. These three detectors provide a choice of BER vs. complexity trade-offs for practical implementations, motivating us to probe further in the quest for even more attractive low-complexity detectors for SM-NOMA systems. Furthermore, low-complexity detection algorithms were proposed for MIMO-NOMA systems [29]–[31] based on the channel input-output relationships represented by a factor graph. The Gaussian message passing-aided (GMP) detectors of [29] reduce the detection complexity of the MPA operating

TABLE I
CONTRASTING THE CONTRIBUTIONS OF THIS WORK TO THE LITERATURE.

Contributions	this work	[14]	[15]	[16]	[27], [28]	[29]	[30]	[31]
SM-NOMA	✓	✓	✓	✓	✓			
MPA detection	✓	✓		✓	✓			
AMP detection	✓					✓	✓	✓
Multicarrier (MC) communications	✓			✓				
Forward error correction (FEC) coding	✓						✓	✓
Capacity analysis	✓							
Complexity analysis	✓				✓	✓	✓	✓

on a fully connected factor graph. In [30], an expectation propagation (EP) framework was applied in the context of the factor graph for reducing the detection complexity of MIMO-NOMA. The Gaussian approximation-based MPA conceived in [31] approximates the discrete interferences encountered at the variable nodes (VNs) of the factor graph by continuous Gaussian-distributed messages. However, the direct application of these algorithms to the family of SM-NOMA systems also leads to significant performance erosion.

Hence, motivated to fill this gap in the literature by conceiving approximate message passing (AMP)-based detectors for the SM-aided SCDMA (SM-SCDMA) system proposed in [16]. The contributions of this paper are boldly and explicitly contrasted to the literature in Table I, which are further elaborated on as follows.

- Firstly, an AMP detector is conceived for SM-SCDMA. Explicitly, the state-of-the-art MPA detector of [16] is complex, because it calculates the exact information conveyed through the factor graph, while the AMP detector approximates the information to be conveyed downward through the factor graph by a Gaussian distribution. This direct application of the AMP detector to the SM-SCDMA system achieves a much lower detection complexity than the MPA detector, albeit at the cost of a degraded BER performance.

- A pair of more sophisticated detectors is conceived for improving the BER performance by exploiting a unique property of SM. Firstly, an enhanced AMP (EAMP) detector is proposed by incorporating a constellation point into the QAM symbol set at zero for representing idle TAs. Furthermore, after an appropriately selected number of iterations, interference cancellation (IC) is embedded into the receiver for reducing the number of edges in the factor graph, when the *a posteriori* probabilities of some of the detected symbols have become sufficiently reliable. The EAMP detector imposes less than 1% complexity of the state-of-the-art MPA detector. Compared to the best-performing FCSD detector of [28] – which achieves 50% complexity reduction compared to the MPA detector – the EAMP detector achieves similar BER performance at a much lower complexity. Additionally, by adopting the classic expectation propagation (EP) principles, a further improved EAMP-EP detector is proposed for reducing the detection complexity of the EAMP detector, albeit this is achieved at the cost of a BER degradation.

- The single-user discrete-input continuous-output memoryless channel (DCMC) capacity of SM-SCDMA is

derived for the first time as the ultimate system capacity bound. Finally, the BER of both the coded and uncoded MPA, AMP, EAMP and EAMP-EP detectors is quantified vs. their complexity.

The rest of this paper is structured as follows. Section II reviews the transceiver structure of SM-SCDMA. Then, the proposed detectors are introduced in Section III, while Section IV characterizes the SM-SCDMA system in terms of its capacity, BER performance and complexity. Finally, Section V offers our conclusions.

II. SM-SCDMA SYSTEM MODEL

In this section, the SM-SCDMA transmitter and receiver are reviewed in Sections II-A and II-B, respectively. Furthermore, main assumptions and notations of this paper are detailed along with the description of the system model.

A. Transmitter Model

The single-cell multiuser uplink (UL) is considered. To be more specific, assume that the system supports U users by relying on N orthogonal resources ($N \leq U$) in the frequency domain, i.e. N orthogonal subcarriers, to simultaneously transmit their signal to the base station (BS) equipped with N_r receive antennas (RAs). For each of the U users, N_t TAs are employed at the transmitter, but only a single TA is activated at each symbol duration (SD). As shown in Fig. 1, after the FEC encoder, the B-bit information stream $\boldsymbol{b}_u$ transmitted by user u is first encoded to the C-bit coded stream $\boldsymbol{c}_u$ and then mapped to $F = C/(\log_2 M)$ number of N_tSSK-M_2QAM symbols $\boldsymbol{x}_u = [x_u^{(1)}, x_u^{(2)}, \cdots, x_u^{(F)}]^T$, where $M = N_t M_2$. Each symbol is then transmitted by one of the N_t UL TAs of user u in a SD. More specifically, the f-th ($f = 1, 2, \cdots, F$) transmit symbol x_u^f is expressed as

$$x_u^{(f)} = t_u^{(f)} | s_u^{(f)}, \tag{1}$$

where $t_u^{(f)}$ is the SSK modulated symbol selected from the SSK symbol set $\mathcal{M}_1 = \{1, \cdots, N_t\}$, while $s_u^{(f)}$ is the QAM symbol selected from the set $\mathcal{M}_2 = \{m_1, m_2, \cdots, m_{M_2}\}$. Now, the SSK-QAM symbol set can be defined as $\mathcal{M} = \mathcal{M}_1 \otimes \mathcal{M}_2 = \{m_{11}, m_{12}, \cdots, m_{N_t M_2}\}$, where $\otimes$ is the Kronecker product [35].

Following this, the f-th QAM symbol $s_u^{(f)}$ of user u is spread across the d_c out of N subcarriers by employing an LDS $\boldsymbol{v}_u = [v_{u1}, v_{u2}, \cdots, v_{uN}]$ preassigned to user u, which has only d_c ($d_c \ll N$) non-zero values and is normalized to satisfy $\|\boldsymbol{v}_u\|^2 = 1$. Hence, the resultant signal of user u
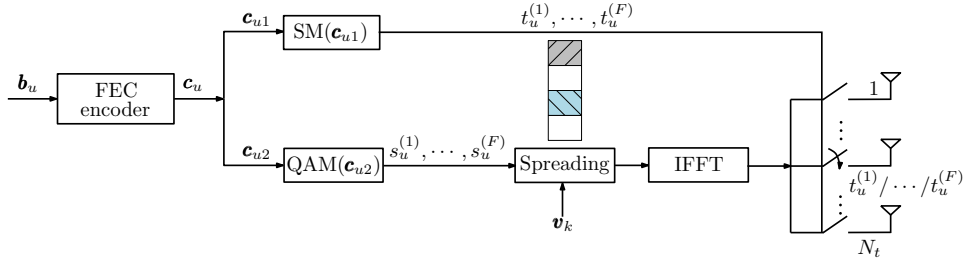
Fig. 1. The transmitter schematic diagram of the u-th user in the SM-SCDMA system.
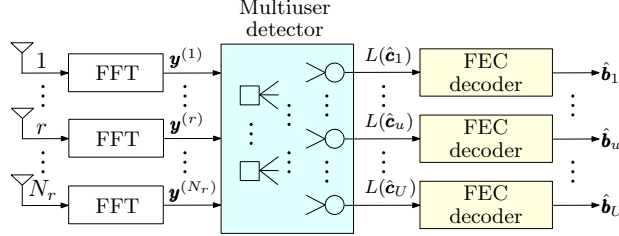
Fig. 2. The UL receiver schematic diagram of the SM-SCDMA system relying on R RAs at BS.

for transmission during the F SDs over the wireless channel by the $t_u^{(1)}$-th, $t_u^{(2)}$-th, $\cdots$, $t_u^{(F)}$-th TA are expressed as $s_u^{(1)}\boldsymbol{v}_u, s_u^{(2)}\boldsymbol{v}_u, \cdots, s_u^{(F)}\boldsymbol{v}_u$, respectively.

B. Receiver Model

Assume that the frequency-selective Rayleigh fading channel has L paths in the time domain (TD) and that the channel state information (CSI) is independent at each SD, which can be achieved with the aid of symbol interleaving [36]. Hence, given the channel impulse response (CIR) between the t-th TA of user u and the r-th RA of BS as

$$\boldsymbol{h}_{t_u}^{(r,f)} = [h_{t_u,1}^{(r,f)}, h_{t_u,2}^{(r,f)}, \cdots, h_{t_u,L}^{(r,f)}]^T,$$
$$t_u = 1, \cdots, N_t, \ r = 1, \cdots, N_r, \ f = 1, \cdots, F, \quad (2)$$

where $\boldsymbol{h}_{t_u}^{(r,f)}$ obeys the complex Gaussian distribution with a zero mean and a variance of $1/2L$ per dimension. The resultant frequency-domain channel transfer function (FDCHTF) experienced by the N subcarriers can be expressed as [36]

$$\hat{\boldsymbol{h}}_{t_u}^{(r,f)} = \boldsymbol{\mathcal{F}}\boldsymbol{\Phi}_L \boldsymbol{h}_{t_u}^{(r,f)}, \quad (3)$$

Then the signal $\boldsymbol{y}^{(r,f)}$ of the N subcarriers received by the r-th RA in the f-th SD can be expressed as

$$\boldsymbol{y}^{(r,f)} = \sum_{u=1}^{U} \mathrm{diag}(\hat{\boldsymbol{h}}_{t_u}^{(r,f)}) s_u^{(f)} \boldsymbol{v}_u + \boldsymbol{z}^{(r,f)}, \quad (4)$$

where $\boldsymbol{z}^{(r,f)}$ is the Gaussian noise vector having a zero mean and a covariance matrix of $2\sigma^2 \boldsymbol{I}_N$, expressed as $\mathcal{CN}(0, 2\sigma^2 \boldsymbol{I}_N)$, with $\sigma^2 = 1/(2\omega_0)$, and ω_0 is the SNR per symbol.

The receiver operates on the basis of log-likelihood ratios (LLRs). More specifically, given the received signal $\boldsymbol{y}^{(r,f)}$ of (4), the *a priori* LLR $L^{(ap)}(c_{p,u}^{(f)})$ and the *extrinsic* LLR $L(c_{p,u}^{(f)})$ of the p-th ($1 \le p \le \log_2 M$) bit of the detected

symbol $\hat{x}_u^{(f)} = \hat{t}_u^{(f)} | \hat{s}_u^{(f)}$, which is entered into the decoder can be expressed as

$$L(\hat{c}_{p,u}^{(f)}) = \ln \frac{\sum_{\hat{x}_u^{(f)} \in \mathcal{B}_{p,u}^{(0)}} p(\hat{x}_u^{(f)} | \boldsymbol{y}^{(f)})}{\sum_{\hat{x}_u^{(f)} \in \mathcal{B}_{p,u}^{(1)}} p(\hat{x}_u^{(f)} | \boldsymbol{y}^{(f)})} - L^{(ap)}(\hat{c}_{p,u}^{(f)}), \quad (5)$$

where $\mathcal{B}_{p,u}^{(0)}$ and $\mathcal{B}_{p,u}^{(1)}$ represent the sub-constellation set of $\mathcal{M}$ that comprises the element having the p-th bit of the constellation point as 0 and 1, respectively, and $p(\hat{x}_u^{(f)} | \boldsymbol{y}^{(f)})$ is the *a posterior* probability of $\hat{x}_u^{(f)}$. Additionally, $L(\hat{\boldsymbol{c}}_u) = \left[L(\hat{c}_{1,u}^{(1)}), \cdots, L(\hat{c}_{\log_2 M,u}^{(F)}) \right]^T$. In order to obtain the *a posterior* probability $p(\hat{x}_u^{(f)} | \boldsymbol{y}^{(f)})$, different detection algorithms will be discussed in Section III.

III. DETECTION ALGORITHMS

In Section III-A, the MPA detector, which was originally proposed in [14] for the SM-SCDMA system, is reviewed. Following this, in Section III-B, low-complexity AMP detection is applied for SM-SCDMA. Then, a pair of novel detection algorithms based on the AMP algorithms are proposed in Sections III-C to III-D, respectively. Note that in this section, the superscript (f) is omitted for simplicity, since the detection operations of all four detectors are identical for different symbols.

A. MPA Detection

The MPA detector was first proposed in [14] for SM-SCDMA systems. It exploits the connections between the N subcarriers and the U users, which can be represented by a factor graph, as exemplified in Fig. 3, and passes the information alongside the edges of the factor graph.

As shown in Fig. 3, the $U = 6$ users represent $U = 6$ variable nodes (VNs), while the $N = 4$ subcarriers are represented by $N = 4$ check nodes (CNs) in the factor
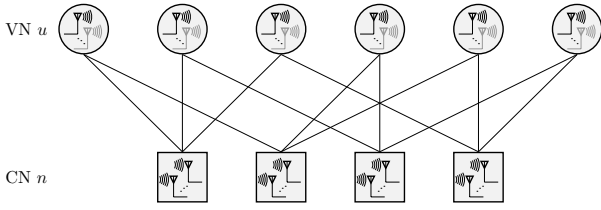
Fig. 3. The factor graph of the SM-SCDMA system supporting $U = 6$ users by $N = 4$ subcarriers.

Algorithm 1: MPA detection in SM-SCDMA [16]

Input

Received signal $\boldsymbol{y}_r$ and $\hat{\boldsymbol{h}}_{t_u}^{(r)}$ for $t = 1, 2, \cdots N_t$,
$r = 1, 2, \cdots, N_r$, $u = 1, 2, \cdots, U$;

Output

The *a posterior* probability $p(\hat{x}_u | \boldsymbol{y})$, $u = 1, \cdots, U$.

Initialization:
$\eta_{u \to n}^{(x_u, 0)} = 1/M$, $x_u \in \mathcal{M}$, $n \in \mathcal{C}_u$, $u = 1, \cdots, U$;

1: **for** $i = 1, \cdots, I$ **do**
2:    **for** $u = 1, \cdots, U$ **do**
3:       Calculate $\delta_{n \to u}^{(x_u, i)}$ for $x_u \in \mathcal{M}$, $n \in \mathcal{C}_u$ using (9);
4:    **end for**
5:    **for** $n = 1, \cdots, N$ **do**
6:       Calculate $\eta_{u \to n}^{(x_u, i)}$ for $x_u \in \mathcal{M}$, $u \in \mathcal{U}_n$ using (10);
7:    **end for**
8: **end for**
9: Calculate the *a posterior* probability $p(\hat{x}_u | \boldsymbol{y})$ using (12) for $u = 1, \cdots, U$.

---

graph. Following the principles of MPA, the information can be propagated both upwards and downwards via the edge $e_{u,n}$, $u = 1, \cdots, U$, $n = 1, \cdots, N$, of the factor graph. Additionally, the CNs connected to the VN u belong to the set $\mathcal{C}_u$ and similarly, the VNs connected to the CN n belong to the set $\mathcal{U}_n$, which are expressed as

$$\mathcal{U}_n = \{u : 1 \leqslant u \leqslant U, e_{u,n} \neq 0\}, n = 1, \cdots, N, \quad (6)$$

$$\mathcal{C}_u = \{n : 1 \leqslant n \leqslant N, e_{u,n} \neq 0, \}, u = 1, \cdots, U. \quad (7)$$

In summary, the MPA detector of the SM-SCDMA system is described by Algorithm 1, which jointly detects the SSK and QAM symbols. More specifically, the initial information $\eta_{u \to n}^{x_u, (0)}$ conveyed from the VN u to the CN n is the *a priori* likelihood of the SSK-QAM symbol $x_u = t_u | s_u \in \mathcal{M}$. Assuming their equiprobable transmission, the initialisation of the MPA detector can be formulated as

$$\eta_{u \to n}^{(x_u, 0)} = 1/M, \ x_u \in \mathcal{M}, u = 1, 2, \cdots, U, \ n = 1, 2, \cdots, N. \quad (8)$$

Then, following the rules of the MPA [16], in the i-th inner iteration, the message $\delta_{n \to u}^{(x_u, i)}$ propagating upwards and $\eta_{u \to n}^{(x_u, i)}$ downwards via the edge $e_{u,n}$ of the factor graph can be expressed respectively as

$$\delta_{n \to u}^{(x_u, i)} = \sum_{\boldsymbol{x}_{[n]} \in \mathcal{M}^{d_c - 1}, x_u} \left(\prod_{x' \in \boldsymbol{x}_{[n]} \backslash x_u} \eta_{u \to n}^{(x', i-1)} \right) \prod_{r=1}^{N_r} p(y_n^{(r)} | \boldsymbol{x}_{[n]}), \quad (9)$$

$$\eta_{u \to n}^{(x_u, i)} = \varepsilon_{u \to n} \prod_{n' \in \mathcal{C}_u \backslash n} \delta_{n' \to u}^{(x_u, i)}, \quad (10)$$

where $\delta_{n \to u}^{(x_u, i)}$ represents the information transmitted from the CN n to the VN u; $\eta_{u \to n}^{(x_u, i)}$ represents information transmitted from the VN u to the CN n, and $\boldsymbol{x}_{[n]}$ represents the symbols sent by the d_u users who share the n-th subcarrier. Additionally, $\mathcal{C}_u \backslash n$ represents the $(d_c - 1)$ subcarriers employed to transmit the symbol except for the n-th subcarrier, and $\boldsymbol{x}_{[n]} \backslash x_u$ represents the $(d_c - 1)$ symbols transmitted by the n-th subcarrier except for x_u. Furthermore, the PDF of $p(y_n | \boldsymbol{x}_{[n]})$ given $\boldsymbol{x}_{[n]}$ can be expressed as

$$p(y_n^{(r)} | \boldsymbol{x}_{[n]}) = \frac{1}{2\pi\sigma^2} \exp \left(-\frac{|y_n^{(r)} - \sum_{u \in \mathcal{U}_n} \hat{h}_{t_u, n}^{(r)} s_u v_{un}|^2}{2\sigma^2} \right). \quad (11)$$

After I iterations, the *a posteriori* probability $p(\hat{x}_u | \boldsymbol{y})$ of $\hat{x}_u$ can be expressed as

$$p(\hat{x}_u | \boldsymbol{y}) = \eta_u^{(x_u, I)} = \prod_{n \in \mathcal{C}_u} \delta_{n \to u}^{(x_u, I)}. \quad (12)$$

The bit LLRs are then calculated from (5) with $p(\hat{x}_u | \boldsymbol{y})$ given in (12).

B. AMP Detection

In contrast to MPA detection, where the information associated with SSK and QAM symbols is propagated jointly via the factor graph, the AMP detector first approximates the likelihood of the QAM symbol $s_u \in \mathcal{M}_2$ conveyed by the t-th TA at the VN u to the r-th RA at the CN n as a complex Gaussian distribution with a mean of $\mu_{tu \to rn}^{(i)}$ and variance of $\tau_{tu \to rn}^{(i)}$, which can be expressed as

$$\mathcal{N}_{\mathbb{C}}(s_u; \mu_{tu \to rn}^{(i)}, \tau_{tu \to rn}^{(i)}) \triangleq \frac{\exp \left(-\frac{|s_u - \mu_{tu \to rn}^{(i)}|^2}{\tau_{tu \to rn}^{(i)}} \right)}{(\pi \tau_{tu \to rn}^{(i)})}. \quad (13)$$

Before detailing AMP detection, let us first define a pair of sets, which represents the VN indices that have connections to the r-th RA at the CN n and the CN indices that have connections to the t-th TA at the VN u, respectively, which are given by

$$\mathcal{U}_{rn} = \{u : 1 \leqslant u \leqslant U, t : 1 \leqslant t \leqslant N_t, e_{tu, rn} \neq 0\},$$
$$n = 1, \cdots, N, r = 1, \cdots, N_r, \quad (14)$$

$$\mathcal{C}_{tu} = \{n : 1 \leqslant n \leqslant N, r : 1 \leqslant r \leqslant N_r, e_{tu, rn} \neq 0, \},$$
$$u = 1, \cdots, U, t = 1, \cdots, N_t. \quad (15)$$

The initialization of $\eta_{tu \to rn}^{(s_u, 0)}$ is expressed as $\eta_{tu \to rn}^{(s_u, 0)} = 1/M$. Then, in the 1-st iteration, the mean $\mu_{tu \to rn}^{(1)}$ and variance $\tau_{tu \to rn}^{(1)}$ of the random variable distribution s_u can be initialized as [37]

$$\mu_{tu \to rn}^{(1)} = \sum_{s_u \in \mathcal{M}_2} s_u \cdot \eta_{tu \to rn}^{(s_u, 0)} = \frac{1}{M} \sum_{s_u \in \mathcal{M}_2} s_u \quad (16)$$

$$\tau_{tu \to rn}^{(1)} = \sum_{s_u \in \mathcal{M}_2} \left| s_u - \mu_{tu \to rn}^{(1)} \right|^2 \cdot \eta_{tu \to rn}^{(s_u, 0)}. \quad (17)$$
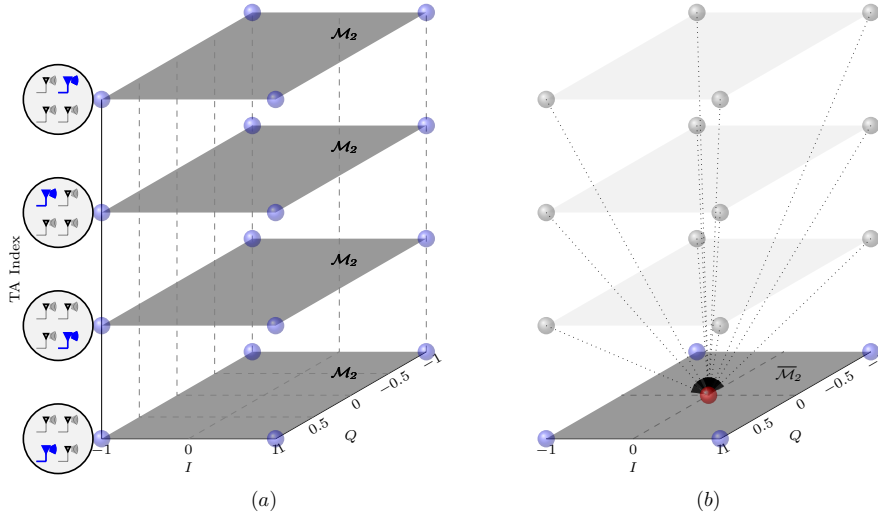
Fig. 4. (a) Conventional SSK-QAM and (b) the proposed integrated constellation $\bar{\mathcal{M}}_2$ for the active TA with $N_t = M_2 = 4$.

Algorithm 2: AMP detection in SM-SCDMA

Input

Received signal $\boldsymbol{y}_r$ and $\hat{\boldsymbol{h}}_{t_u}^{(r)}$ for $t = 1, 2, \cdots, N_t$, $r = 1, 2, \cdots, N_r$, $u = 1, 2, \cdots, U$;

Output

The *a posterior* probability $p(\hat{x}_u|\boldsymbol{y})$, $u = 1, \cdots, U$.

Initialization:

$\eta_{tu \to rn}^{(s_u, 0)} = 1/M$, $s_u \in \mathcal{M}_2$, $rn \in \mathcal{C}_{tu}$, $t = 1, 2, \cdots, N_t$, $r = 1, 2, \cdots, N_r$, $n = 1, 2, \cdots, N$, $u = 1, 2, \cdots, U$.

1: **for** $i = 1, \cdots, I$ **do**
2:   **for** $r = 1, 2, \cdots, N_r$, $n = 1, 2, \cdots, N$ **do**
3:     Calculate $\mu_{tu \to rn}^{(i)}$ and $\tau_{tu \to rn}^{(i)}$ for $tu \in \mathcal{U}_{rn}$, using (25) and (26);
4:   **end for**
5:   **for** $t = 1, 2, \cdots, N_t$, $u = 1, 2, \cdots, U$ **do**
6:     Calculate $\alpha_{rn \to tu}^{(i)}$ and $\beta_{rn \to tu}^{(i)}$ for $rn \in \mathcal{C}_{tu}$, using (19) and (20);
7:   **end for**
8:   **for** $r = 1, 2, \cdots, N_r$, $n = 1, 2, \cdots, N$ **do**
9:     Calculate
$$\eta_{tu \to rn}^{(s_u, i)} = \frac{\mathcal{N}_{\mathbb{C}}\left(s_u; \xi_{tu \to rn}^{(i)}, \gamma_{tu \to rn}^{(i)}\right)}{\sum_{t' \in \mathcal{M}_1, s_u' \in \mathcal{M}_2} \mathcal{N}_{\mathbb{C}}\left(s_u'; \xi_{t'u \to rn}^{(i)}, \gamma_{t'u \to rn}^{(i)}\right)}$$ for $tu \in \mathcal{U}_{rn}$, using (23) and (24), with $s_u \in \mathcal{M}_2$;
10:   **end for**
11: **end for**
12: Calculate $p(\hat{x}_u|\boldsymbol{y}) = \eta_{tu}^{(s_u, I)} = \frac{\mathcal{N}_{\mathbb{C}}\left(s_u; \xi_{tu}^{(I)}, \gamma_{tu}^{(I)}\right)}{\sum_{s_u' \in \bar{\mathcal{M}}_2} \mathcal{N}_{\mathbb{C}}\left(s_u'; \xi_{tu}^{(I)}, \gamma_{tu}^{(I)}\right)}$ using (27) and (28) with $s_u \in \mathcal{M}_2$, for $t \in \mathcal{M}_1$, $u = 1, \cdots, U$.

Later in the i-th iteration, the upward information propagation $\delta_{rn \to tu}^{(s_u, i)}$ from the CN rn to the VN tu can be expressed as

$$\delta_{rn \to tu}^{(s_u, i)} = \sum_{\boldsymbol{x}_{[rn]} \backslash t_u | s_u} \left(\prod_{t'u' \in [rn] \backslash tu} \mathcal{N}_{\mathbb{C}}(s_{u'}; \mu_{t'u' \to rn}^{(i)}, \tau_{t'u' \to rn}^{(i)}) \right)$$
$$\times p(y_n^{(r)}|\boldsymbol{x}_{[rn]}, t_u|s_u) \tag{18a}$$
$$= \mathcal{N}_{\mathbb{C}}\left(\hat{h}_{t_u, n}^{(r)} s_u; \alpha_{rn \to tu}^{(i)}, \beta_{rn \to tu}^{(i)}\right), \tag{18b}$$

where $\alpha_{rn \to tu}^{(i)}$ and $\beta_{rn \to tu}^{(i)}$ are the mean $\alpha_{rn \to tu}^{(i)}$ and variance $\beta_{rn \to tu}^{(i)}$ of the variable $\hat{h}_{t_u, n}^{(r)} s_u$, respectively, which can be expressed as

$$\alpha_{rn \to tu}^{(i)} = y_n^{(r)} - \sum_{t'u' \in \mathcal{U}_{rn} \backslash tu} \hat{h}_{t'_{u'}, n}^{(r)} \mu_{t'u' \to rn}^{(i)} \tag{19}$$

and

$$\beta_{rn \to tu}^{(i)} = \omega_0 + \sum_{t'u' \in \mathcal{U}_{rn} \backslash tu} |\hat{h}_{t'_{u'}, n}^{(r)}|^2 \tau_{t'u' \to rn}^{(i)}. \tag{20}$$

Meanwhile, the downward information propagation from the CN n to the VN u is the same as that employed in the MPA detector, which can be expressed as

$$\eta_{tu \to rn}^{(s_u, i)} = \varepsilon_{tu \to rn} \prod_{r'n' \in \mathcal{C}_{tu} \backslash rn} \delta_{r'n' \to tu}^{(i)}. \tag{21}$$

Then by substituting $\delta_{rn \to tu}^{s_u, (i)} = \mathcal{N}_{\mathbb{C}}\left(\hat{h}_{t_u, n}^{(r)} s_u; \alpha_{rn \to tu}^{(i)}, \beta_{rn \to tu}^{(i)}\right)$ into (21), we have

$$\eta_{tu \to rn}^{(s_u, i)} = \frac{\mathcal{N}_{\mathbb{C}}\left(s_u; \xi_{tu \to rn}^{(i)}, \gamma_{tu \to rn}^{(i)}\right)}{\sum_{t' \in \mathcal{M}_1, s_u' \in \mathcal{M}_2} \mathcal{N}_{\mathbb{C}}\left(s_u'; \xi_{t'u \to rn}^{(i)}, \gamma_{t'u \to rn}^{(i)}\right)}, \tag{22}$$

where the variance $\gamma_{tu \to rn}^{(i)}$ and the mean $\xi_{tu \to rn}^{(i)}$ are expressed as

$$\gamma_{tu \to rn}^{(i)} = \left(\sum_{r'n' \in \mathcal{C}_{tu} \backslash rn} \frac{|\hat{h}_{t_u, n}^{(r')}|^2}{\beta_{r'n' \to tu}^{(i)}} \right)^{-1} \tag{23}$$

and

$$\xi_{tu \to rn}^{(i)} = \gamma_{tu \to rn}^{(i)} \sum_{r'n' \in \mathcal{C}_{tu} \setminus rn} \frac{\hat{h}_{t_u,n}^{*(r')} \alpha_{r'n' \to tu}^{(i)}}{\beta_{r'n' \to tu}^{(i)}}, \qquad (24)$$

respectively.

In order to find the Gaussian approximate $\tilde{\eta}_{tu \to rn}^{(s_u,i)}$ of $\eta_{tu \to rn}^{(s_u,i)}$, a natural approach is to minimize the inclusive Kullback-Leibler (KL) divergence $\text{KL}\left(\eta_{tu \to rn}^{(s_u,i)} \| \tilde{\eta}_{tu \to rn}^{(s_u,i)}\right)$ [37], which gives

$$\mu_{tu \to rn}^{(i)} = \sum_{s_u \in \mathcal{M}_2} s_u \cdot \eta_{tu \to rn}^{(s_u,i-1)} \qquad (25)$$

$$\tau_{tu \to rn}^{(i)} = \sum_{s_u \in \mathcal{M}_2} |s_u - u_{tu \to rn}^{(i)}|^2 \cdot \eta_{tu \to rn}^{(s_u,i-1)}. \qquad (26)$$

At the final iteration, the message received at the VN tu is approximated as $\eta_{tu}^{(s_u,I)} = \mathcal{N}_{\mathbb{C}}\left(s_u; \xi_{tu}^{(I)}, \gamma_{tu}^{(I)}\right)$, where the mean $\xi_{tu}^{(I)}$ and variance $\gamma_{tu}^{(I)}$ are calculated as

$$\xi_{tu}^{(I)} = \left(\sum_{r'n' \in \mathcal{C}_{tu}} \frac{|\hat{h}_{t_u,n}^{(r')}|^2}{\beta_{r'n' \to tu}^{(I)}} \right)^{-1} \qquad (27)$$

and

$$\gamma_{tu}^{(I)} = \gamma_{tu}^{(I)} \sum_{r'n' \in \mathcal{C}_{tu}} \frac{\hat{h}_{t_u,n}^{*(r')} \alpha_{r'n' \to tu}^{(I)}}{\beta_{r'n' \to tu}^{(I)}}, \qquad (28)$$

respectively. After the normalization, the *a posteriori* probability $p(\hat{x}_u | \boldsymbol{y})$ of $\hat{x}_u$ is expressed as

$$p(\hat{x}_u | \boldsymbol{y}) = \eta_{tu}^{(s_u,I)} = \frac{\mathcal{N}_{\mathbb{C}}\left(s_u; \xi_{tu}^{(I)}, \gamma_{tu}^{(I)}\right)}{\sum_{t' \in \mathcal{M}_1, s'_u \in \mathcal{M}_2} \mathcal{N}_{\mathbb{C}}\left(s'_u; \xi_{t'u}^{(I)}, \gamma_{t'u}^{(I)}\right)}. \qquad (29)$$

When $p(\hat{x}_u | \boldsymbol{y})$ of all F symbols are obtained, the *extrinsic* LLRs $L(\hat{\boldsymbol{c}}_u)$ entered into the FEC decoder will be calculated using (5) with $p(\hat{x}_u | \boldsymbol{y})$ given in (29).

C. EAMP Detection

The enhanced AMP (EAMP) detector exploits the unique properties of SM-SCDMA systems, for outperforming the AMP detector, by relying the following two aspects:

1) Integrated symbol constellation: Since only one of the N_t TAs is activated within a single SD, an extra symbol $s_u = 0$ is introduced for representing that the t-th TA of user u remains idle at the current SD. Specifically, the SSK-QAM set $\mathcal{M}$ can be illustrated by Fig. 4(a). When the inactive TAs are represented by zeros, the integrated QAM symbol constellation representing the active TA of user u becomes $\bar{\mathcal{M}}_2 = \mathcal{M}_2 \cup 0$, as exemplified in Fig. 4(b), where $N_t = M_2 = 4$. More specifically, as shown in Fig. 4(b), when $\eta_{tu \to rn}^{(s_u,i)}$ is updated during the i-th iteration of the EAMP detector, where $t = 4$, (M_2+1) symbol possibilities are calculated for each $s_u \in \bar{\mathcal{M}}_2$.

Correspondingly, the mean $\mu_{tu \to rn}^{(i)}$ and variance $\tau_{tu \to rn}^{(i)}$ of the Gaussian distribution $\mathcal{N}_{\mathbb{C}}(s_u; \mu_{tu \to rn}^{(i)}, \tau_{tu \to rn}^{(i)})$, where

$s_u \in \bar{\mathcal{M}}_2$, are expressed as

$$\mu_{tu \to rn}^{(i)} = \sum_{s_u \in \bar{\mathcal{M}}_2} s_u \cdot \eta_{tu \to rn}^{(s_u,i-1)}, \qquad (30)$$

$$\tau_{tu \to rn}^{(i)} = \sum_{s_u \in \bar{\mathcal{M}}_2} |s_u - \mu_{tu \to rn}^{(i)}|^2 \cdot \eta_{tu \to rn}^{(s_u,i-1)}. \qquad (31)$$

Additionally, the normalization process of (22) for $s_u \in \bar{\mathcal{M}}_2$ now becomes

$$\eta_{tu \to rn}^{(s_u,i)} = \frac{\mathcal{N}_{\mathbb{C}}\left(s_u; \xi_{tu \to rn}^{(i)}, \gamma_{tu \to rn}^{(i)}\right)}{\sum_{s'_u \in \bar{\mathcal{M}}_2} \mathcal{N}_{\mathbb{C}}\left(s'_u; \xi_{tu \to rn}^{(i)}, \gamma_{tu \to rn}^{(i)}\right)}, s_u \in \bar{\mathcal{M}}_2. \qquad (32)$$

Finally, after I iterations we have

$$p(\hat{x}_u | \boldsymbol{y}) = \eta_{tu}^{(s_u,I)} = \frac{\mathcal{N}_{\mathbb{C}}\left(s_u; \xi_{tu}^{(I)}, \gamma_{tu}^{(I)}\right)}{\sum_{s'_u \in \bar{\mathcal{M}}_2} \mathcal{N}_{\mathbb{C}}\left(s'_u; \xi_{tu}^{(I)}, \gamma_{tu}^{(I)}\right)}, s_u \in \mathcal{M}_2. \qquad (33)$$

Now the *extrinsic* LLRs $L(\hat{\boldsymbol{c}}_u)$ entered into the FEC decoder are calculated using (5) with $p(\hat{x}_u | \boldsymbol{y})$ given by (33).

2) Threshold-aided Interference Cancellation (IC): After a sufficiently high number of AMP iterations, the *a posteriori* probabilities of some VNs become highly reliable, hence they would only be improved very marginally in the following iterations. Therefore, the detection complexity can be further reduced by invoking IC for cancelling some edges of the factor graph.

Specifically, after every ϱ iterations, where ϱ may either be constant or adapted during the iterative detection, *a posteriori* probability $p(\hat{x}_u | \boldsymbol{y}) = \eta_{tu}^{(s_u,i)}$ of $\hat{x}_u$ in the current i-th iteration is calculated using (29) with $s_u \in \mathcal{M}_2$ and substituting I with i. If $\eta_{tu}^{(s_u,i)}$ is higher than a certain pre-set threshold P_{th}, i.e., $\eta_{tu}^{(s_u,i)} > P_{\text{th}}$, then it indicates that the detected symbol $t_u | s_u$ has a reliability higher than P_{th}, so $\mu_{tu}^{(i)} = s_u$ is set. In the meantime, since the active TA has been identified as t_u, the symbol transmitted by the remaining $(N_t - 1)$ TAs will be 0.

After obtaining $\eta_{tu}^{(s_u,i)} > P_{\text{th}}$, IC is performed to obtain the residual interference $z_{rn}^{(i)}$, which can be expressed as

$$z_{rn}^{(i)} = z_{rn}^{(i-\varrho)} - \hat{h}_{t_u,n}^{(r)} \mu_{tu}^{(i-\varrho)}, \quad \varrho \leq i \leq I, \qquad (34)$$

where $z_{rn}^{(0)} = y_{rn}$. Meanwhile, the corresponding edges $e_{tu,rn}$, $rn \in \mathcal{C}_{tu}$, which are employed to compute $\eta_{tu}^{(s_u,i)}$, are cancelled as well by setting $e_{tu,rn} = 0$.

The operations of the proposed EAMP detector are summarized in Algorithm 3.

D. EAMP-EP Detection

As discussed in Section III-C, the calculation of $\eta_{tu \to rn}^{(s_u,i)}$ using (32) is performed for all connections to VN u and for all $s_u \in \bar{\mathcal{M}}_2$, which still requires a relatively high detection complexity. For avoiding the calculation of (32) for each connection in the factor graph, the EP algorithm of [37], [38] is adopted, which approximates the symbol belief $\rho_{tu}^{(s_u,i)}$ of s_u

---

Algorithm 3: EAMP detection in SM-SCDMA

Input

Received signal $\boldsymbol{y}_r$ and $\hat{\boldsymbol{h}}_{t_u}^{(r)}$ for $t = 1, 2, \cdots N_t$, $r = 1, 2, \cdots, N_r$, $u = 1, 2, \cdots, U$;

Output

The *a posterior* probability $p(\hat{x}_u|\boldsymbol{y})$, $u = 1, 2, \cdots, U$.

Initialization:

$z_{rn}^{(0)} = y_{rn}$, $\eta_{tu \to rn}^{(s_u, 0)} = 1/M$, $s_u \in \mathcal{M}_2$, $\eta_{tu \to rn}^{(s_u=0,0)} = 1 - 1/N_t$, $rn \in \mathcal{C}_{tu}$, $t = 1, 2, \cdots N_t$, $r = 1, 2, \cdots, N_r$, $n = 1, 2, \cdots, N$, $u = 1, 2, \cdots, U$.

1: **for** $i = 1, \cdots, I$ **do**
2:   **for** $tu \in \mathcal{U}_{rn}$, $r = 1, 2, \cdots, N_r$, $n = 1, 2, \cdots, N$ **do**
3:     Calculate $\mu_{tu \to rn}^{(i)}$ and $\tau_{tu \to rn}^{(i)}$ using (30) and (31) with $s_u \in \mathcal{M}_2$;
4:   **end for**
5:   **for** $t = 1, 2, \cdots N_t$, $u = 1, 2, \cdots, U$ **do**
6:     Calculate $\alpha_{rn \to tu}^{(i)}$ and $\beta_{rn \to tu}^{(i)}$ for $rn \in \mathcal{C}_{tu}$, using (19) and (20);
7:   **end for**
8:   **for** $tu \in \mathcal{U}_{rn}$, $r = 1, 2, \cdots, N_r$, $n = 1, 2, \cdots, N$ **do**
9:     Calculate $\eta_{tu \to rn}^{(s_u, i)} = \dfrac{\mathcal{N}_{\mathbb{C}}\left(s_u; \xi_{tu \to rn}^{(i)}, \gamma_{tu \to rn}^{(i)}\right)}{\sum_{s'_u \in \bar{\mathcal{M}}_2} \mathcal{N}_{\mathbb{C}}\left(s'_u; \xi_{tu \to rn}^{(i)}, \gamma_{tu \to rn}^{(i)}\right)}$ using (23) and (24) with $s_u \in \bar{\mathcal{M}}_2$;
10:   **end for**
11:   **if** $\mathrm{mod}(i, \varrho) == 0$ **then**
12:     **for** $u = 1, 2, \cdots, U$ **do**
13:       Calculate $\eta_{tu}^{(s_u, i)}$ using (29) with $t = 1, 2, \cdots N_t$, substituting I with i;
14:       **if** $\eta_{tu}^{(s_u, i)} > P_{\mathrm{th}}$ AND $s_u \in \mathcal{M}_2$ **then**
15:         $\mu_{tu}^{(i)} = s_u$;
16:         **for** $rn \in \mathcal{C}_{tu}$ **do**
17:           $z_{rn}^{(i)} = z_{rn}^{(i-\varrho)} - \hat{h}_{t_u, n}^{(r)} \mu_{tu}^{(i-\varrho)}$;
18:           $e_{tu, rn} = 0$;
19:         **end for**
20:       **end if**
21:     **end for**
22:   **end if**
23: **end for**
24: Calculate $p(\hat{x}_u|\boldsymbol{y}) = \eta_{tu}^{(s_u, I)} = \dfrac{\mathcal{N}_{\mathbb{C}}\left(s_u; \xi_{tu}^{(I)}, \gamma_{tu}^{(I)}\right)}{\sum_{s'_u \in \bar{\mathcal{M}}_2} \mathcal{N}_{\mathbb{C}}\left(s'_u; \xi_{tu}^{(I)}, \gamma_{tu}^{(I)}\right)}$ using (27) and (28) with $s_u \in \bar{\mathcal{M}}_2$, for $t \in \mathcal{M}_1$, $u = 1, \cdots, U$.

Algorithm 4: EAMP-EP detection in SM-SCDMA

Input

Received signal $\boldsymbol{y}_r$ and $\hat{\boldsymbol{h}}_{t_u}^{(r)}$ for $t = 1, 2, \cdots N_t$, $r = 1, 2, \cdots, N_r$, $u = 1, 2, \cdots, U$;

Output

The *a posterior* probability $p(\hat{x}_u|\boldsymbol{y})$, $u = 1, \cdots, U$.

Initialization:

$z_{rn}^{(0)} = y_{rn}$, $\eta_{tu \to rn}^{(s_u, 0)} = 1/M$, $s_u \in \mathcal{M}_2$, $\eta_{tu \to rn}^{(s_u=0,0)} = 1 - 1/N_t$, $\alpha_{rn \to tu}^{(0)} = 0$, $\beta_{rn \to tu}^{(0)} = \infty$, $rn \in \mathcal{C}_{tu}$, $t = 1, 2, \cdots N_t$, $r = 1, 2, \cdots, N_r$, $n = 1, 2, \cdots, N$, $u = 1, 2, \cdots, U$.

1: **for** $i = 1, \cdots, I$ **do**
2:   **for** $r = 1, 2, \cdots, N_r$, $n = 1, 2, \cdots, N$ **do**
3:     Calculate $\mu_{tu \to rn}^{(i)}$ and $\tau_{tu \to rn}^{(i)}$ for $tu \in \mathcal{U}_{rn}$, using (37) and (38);
4:   **end for**
5:   **for** $t = 1, 2, \cdots, N_t$, $u = 1, 2, \cdots, U$ **do**
6:     Calculate $\alpha_{rn \to tu}^{(i)}$ and $\beta_{rn \to tu}^{(i)}$ for $rn \in \mathcal{C}_{tu}$, using (19) and (20);
7:   **end for**
8:   **if** $\mathrm{mod}(i, \varrho) == 0$ **then**
9:     **for** $u = 1, 2, \cdots, U$ **do**
10:       Calculate $\eta_{tu}^{(s_u, i)}$ using (29) with $s_u \in \bar{\mathcal{M}}_2$, $t = 1, 2, \cdots N_t$, substituting I with i;
11:       Update $\tilde{\mu}_{tu}$ and $\tilde{\tau}_{tu}$ using (39) and (40) with $s_u \in \bar{\mathcal{M}}_2$;
12:       **if** $\eta_{tu}^{(s_u, i)} > P_{\mathrm{th}}$ AND $s_u \in \mathcal{M}_2$ **then**
13:         $\mu_{tu}^{(i)} = s_u$;
14:         **for** $rn \in \mathcal{C}_{tu}$ **do**
15:           $z_{rn}^{(i)} = z_{rn}^{(i-\varrho)} - \hat{h}_{t_u, n}^{(r)} \mu_{tu}^{(i-\varrho)}$;
16:           $e_{tu, rn} = 0$;
17:         **end for**
18:       **end if**
19:     **end for**
20:   **end if**
21: **end for**
22: Calculate $p(\hat{x}_u|\boldsymbol{y}) = \eta_{tu}^{(s_u, I)} = \dfrac{\mathcal{N}_{\mathbb{C}}\left(s_u; \xi_{tu}^{(I)}, \gamma_{tu}^{(I)}\right)}{\sum_{s'_u \in \bar{\mathcal{M}}_2} \mathcal{N}_{\mathbb{C}}\left(s'_u; \xi_{tu}^{(I)}, \gamma_{tu}^{(I)}\right)}$ using (27) and (28) with $s_u \in \bar{\mathcal{M}}_2$, for $t \in \mathcal{M}_1$, $u = 1, \cdots, U$.

---

as Gaussian distribution. More specifically, the symbol belief of s_u is defined as

$$\rho_{tu}^{(s_u, i)} = \frac{\prod_{rn \in \mathcal{C}_{tu}} \delta_{rn \to tu}^{(s_u, i)}}{\sum_{t' \in \mathcal{M}_1, s'_u \in \mathcal{M}_2} \prod_{rn \in \mathcal{C}_{tu}} \delta_{rn \to t'u}^{(s'_u, i)}}. \quad (35)$$

Then the Gaussian approximation of the symbol belief $\rho_{tu}^{(s_u, i)}$ is employed to compute the downward information propagation $\eta_{tu \to rn}^{(s_u, i)}$ of the proposed EAMP detection, which can be expressed as

$$\eta_{tu \to rn}^{(s_u, i)} = \mathcal{N}_{\mathbb{C}}\left(s_u; \mu_{tu \to rn}^{(i)}, \tau_{tu \to rn}^{(i)}\right), \quad (36)$$

where $\mu_{tu \to rn}^{(i)}$ and $\tau_{tu \to rn}^{(i)}$ are the mean and variance of the Gaussian distribution, respectively. According to [30], [37], the mean $\mu_{tu \to rn}^{(i)}$ and variance $\tau_{tu \to rn}^{(i)}$ can be derived using the canonical form of the Gaussian PDF [39], which are expressed respectively as

$$\tau_{tu \to rn}^{(i)} = \left(\frac{1}{\tilde{\tau}_{tu}} - \frac{|\hat{h}_{t_u, n}^{(r)}|^2}{\beta_{rn \to tu}^{(i-1)}}\right)^{-1}, \quad (37)$$

$$\mu_{tu \to rn}^{(i)} = \tau_{tu \to rn}^{(i)} \left(\frac{\tilde{u}_{tu}}{\tilde{\tau}_{tu}} - \frac{\hat{h}_{t_u, n}^{*(r)} \alpha_{rn \to tu}^{(i-1)}}{\beta_{rn \to tu}^{(i-1)}}\right), \quad (38)$$

where $\tilde{\mu}_{tu}$ and $\tilde{\tau}_{tu}$ could still be calculated by using the KL

divergence, expressed as

$$\tilde{\mu}_{tu} = \sum_{s_u \in \bar{\mathcal{M}}_2} s_u \cdot \eta_{tu}^{(s_u,i)} \qquad (39)$$

$$\tilde{\tau}_{tu} = \sum_{s_u \in \bar{\mathcal{M}}_2} |s_u - \tilde{\mu}_{tu}|^2 \cdot \eta_{tu}^{(s_u,i)}. \qquad (40)$$

In summary, the EAMP-EP detector of the SM-SCDMA system is formally defined by Algorithm 4.

IV. PERFORMANCE ANALYSIS

In Section IV-A, the single-user DCMC capacity of the SM-SCDMA system is derived. Then, the performance of the SM-SCDMA system employing the MPA, AMP, EAMP and EAMP-EP detectors are compared in terms of their BER performance and complexity in Section IV-B and IV-C, respectively.

A. DCMC capacity

Let us first derive the DCMC capacity per subcarrier per user. Since the single user case is considered, the subscript $'u'$ is omitted for simplicity. According to [40], the DCMC capacity can be expressed as

$$C_{\text{DCMC}} = \frac{1}{d_c} \sum_{n \in \mathcal{C}} \max_{p(y_n^{(r)}|x), x \in \mathcal{M}} \sum_{r=1}^{N_r} \sum_{x \in \mathcal{M}} \int_{-\infty}^{+\infty} p(y_n^{(r)}, x)$$
$$\times \log_2 \left(\frac{p(y_n^{(r)}|x)}{\sum_{x' \in \mathcal{M}} p(y_n^{(r)}, x')} \right) dy_n, \qquad (41)$$

where $\mathcal{C}$ represents the set of connections between the user and those specific d_c subcarriers that this user's signal spread over. Furthermore, $p(y_n^{(r)}|x)$ is given by (11) and $x \in \mathcal{M}$ represents the specific SSK-QAM symbol that is transmitted by the n-th subcarrier. Note that (41) is maximised in the case of equiprobable transmitted symbols, where $p(x) = 1/(M)$, $x \in \mathcal{M}$. Hence, we arrive at

$$\log_2 \left(\frac{p(y_n^{(r)}|x)}{\sum_{x' \in \mathcal{M}} p(y_n^{(r)}, x')} \right) = \log_2 \left(\frac{p(y_n^{(r)}|x)}{\sum_{x' \in \mathcal{M}} p(y_n^{(r)}|x')p(x')} \right)$$
$$= -\log_2 \left(\frac{1}{M} \sum_{x' \in \mathcal{M}} \frac{p(y_n^{(r)}|x)}{p(y_n^{(r)}|x')} \right)$$
$$= \log_2(M) - \log_2 \sum_{x' \in \mathcal{M}} \exp(\Psi), \qquad (42)$$

where by substituting (11) into (42), Ψ is expressed as

$$\Psi = \frac{-\left| \left(\hat{h}_{t,n}^{(r)} s - \hat{h}_{t',n}^{(r)} s' \right) + z_n^{(r)} \right|^2 + \left| z_n^{(r)} \right|^2}{\sigma^2}, \qquad (43)$$

with $\hat{h}_{t,n}^{(r)}$ representing the channel gain of the n-th subcarrier between the t-th TA and r-th RA, while $z_n^{(r)}$ is the n-th element in the vector $\boldsymbol{z}^{(r)}$.
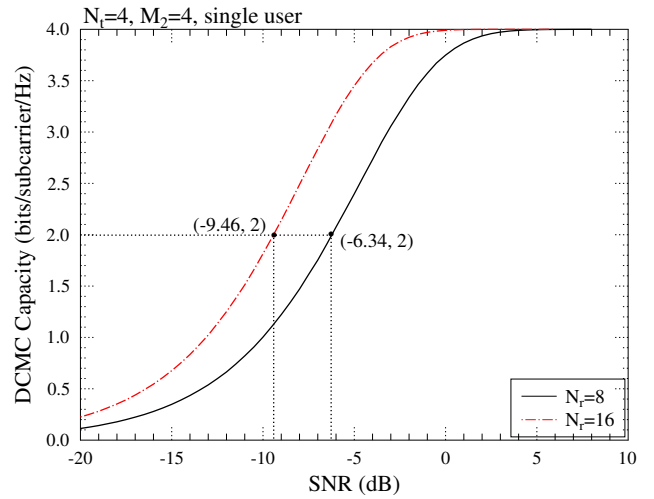
Fig. 5. The single-user DCMC capacity of the SM-SCDMA system having $N_t = 4$, $M_2 = 4$, where $N_r = 8$ and 16 are employed.

Hence, if the symbols are transmitted at equal probabilities, the DCMC capacity per user per subcarrier is expressed as

$$C_{\text{DCMC}} = \frac{1}{d_c} \sum_{n \in \mathcal{C}} \left(\log_2 M - \frac{1}{M} \sum_{x \in \mathcal{M}} \mathbb{E}_{\hat{\boldsymbol{h}}, \boldsymbol{z}} \left[\log_2 \sum_{x' \in \mathcal{M}} \exp(\Psi) \right] \right). \qquad (44)$$

Fig. 5 shows the DCMC capacity of the SM-SCDMA system given by (44) using $N_t = 4$, $M_2 = 4$, $N_r = 8$ or 16 RAs. It may be observed that the asymptotic capacity of the SM-SCDMA system in this case is 4 bits per channel use (bpcu), regardless of the number of RAs. This is consistent with the conclusions of [40], which demonstrated that when the number of RAs is higher than that of the TAs, the increase of RAs will not lead to an increased asymptotic DCMC capacity, even though a higher receive diversity order can be obtained. Furthermore, the half-rate coded single-user SM-SCDMA systems employing $N_r = 16$ and $N_r = 8$ RAs are upper-bounded by a DCMC capacity of 2 bpcu at an SNR of -9.46 and -6.34 dB, respectively.

B. BER Performance

In this section, the BER performance of SM-SCDMA employing different detectors discussed in Section III is investigated, when communicating over frequency-selective Rayleigh fading channels having $L = 4$ paths, with $I = 9$ for the MPA detector and $I = 15$ for the AMP-based detectors, $\varrho = 5$ and $N = 16$ adopted for all simulation results.

First, the uncoded BER performance of the MPA, AMP, EAMP and EAMP-EP detectors for the SM-SCDMA system with $N = 16$ and $U = 24$ is compared, where each user is equipped with $N_t = 4$ TAs, and $N_r = 8$ or 16 RAs are employed at the BS, when communicating over frequency-selective channels having $L = 4$ paths, as shown in Figs. 6 and 7, respectively. Furthermore, the single-user performance
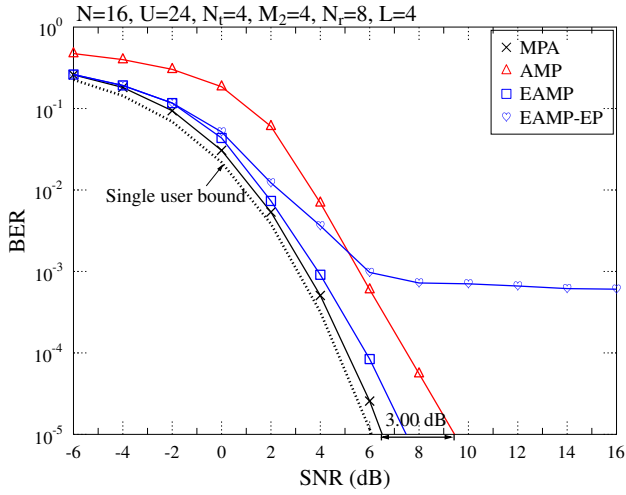
Fig. 6. The uncoded BER performance of the $N = 16, U = 24$ SM-SCDMA system with $N_t = 4$, $N_r = 8$ and $M_2 = 4$, when communicating over $L = 4$ frequency-selective Rayleigh fading channels, where the MPA, AMP, EAMP or EAMP-EP ($P_{th} = 0.99$) detector is employed. The throughput is 6 bpcu.
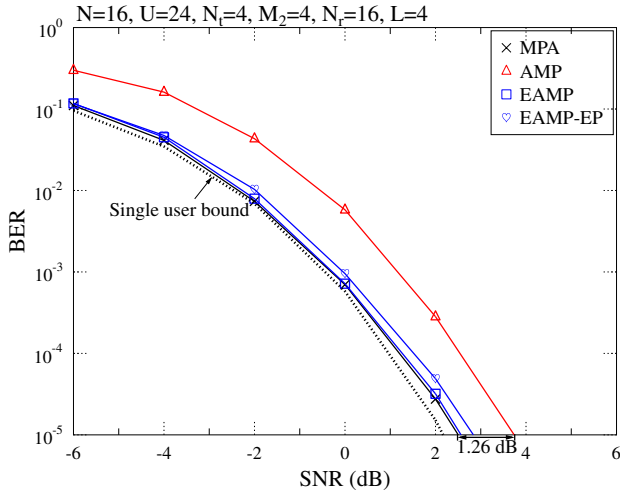
Fig. 7. The uncoded BER performance of the $N = 16, U = 24$ SM-SCDMA system with $N_t = 4$, $N_r = 16$ and $M_2 = 4$, when communicating over $L = 4$ frequency-selective Rayleigh fading channels, where the MPA, AMP, EAMP or EAMP-EP ($P_{th} = 0.99$) detector is employed. The throughput is 6 bpcu.

of the SM-SCDMA system employing full-search-based maximum likelihood detection is also included as our benchmark. It can be readily observed from Fig. 6 that while the AMP detector shows 3 dB performance loss compared to the MPA detector proposed in [16] at a BER of 10^{-4}, the EAMP detector mitigates this performance loss to 1 dB at a BER of 10^{-4}. However, this 2 dB performance improvement of the EAMP detector is achieved at a similar detection complexity to that of the AMP detector, as it will be demonstrated in Section IV-C. Additionally, when the symbol probability exchanged throughout the factor graph is replaced by the approximation of symbol belief given by (35), as in the proposed EAMP-EP detector, the BER performance shows an error-floor formation.
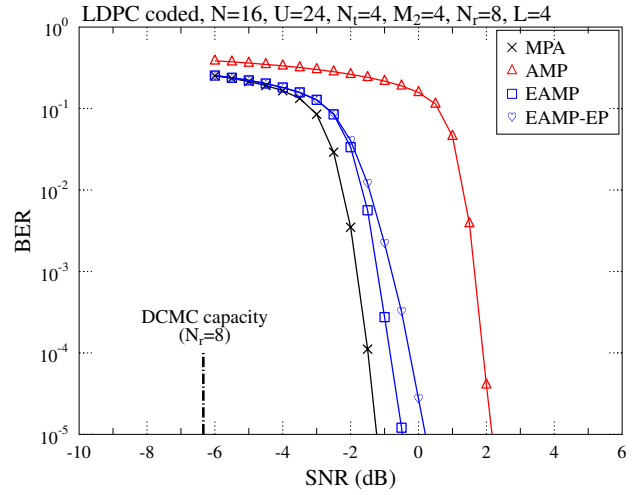
Fig. 8. The half-rate LDPC-coded BER performance of the $N = 16$, $U = 24$ SM-SCDMA system with $N_t = 4$, $N_r = 8$ and $M_2 = 4$, when communicating over $L = 4$ frequency-selective Rayleigh fading channels, where the MPA, AMP, EAMP or EAMP-EP ($P_{th} = 0.99$) detector is employed. The throughput is 3 bpcu.

A potential solution for mitigating the error floor of the EP algorithm is to increase the receive diversity by increasing the number of RAs, as shown in Fig. 7, where the BER performance of the EAMP-EP detector approaches that of the EAMP detector, when $N_r = 16$ RAs are employed. By comparing Figs. 6 and 7, the increase of the number of RAs from $N_r = 8$ to $N_r = 16$ attains over 5 dB SNR gain at a BER of 10^{-5} when employing the EAMP detector.
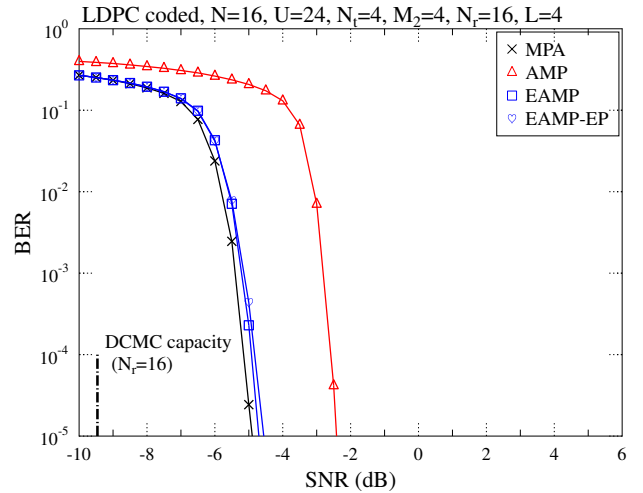
Fig. 9. The half-rate LDPC-coded BER performance of the $N = 16$, $U = 24$ SM-SCDMA system with $N_t = 4$, $N_r = 16$ and $M_2 = 4$, when communicating over $L = 4$ frequency-selective Rayleigh fading channels, where the MPA, AMP, EAMP or EAMP-EP ($P_{th} = 0.99$) detector is employed. The throughput is 3 bpcu.

An alternative way of eliminating this error-floor is the employment of FEC, as shown in Figs. 8 and 9, where the BER performance of the half-rate low-density parity-check (LDPC)-coded SM-SCDMA system employing the same parameters
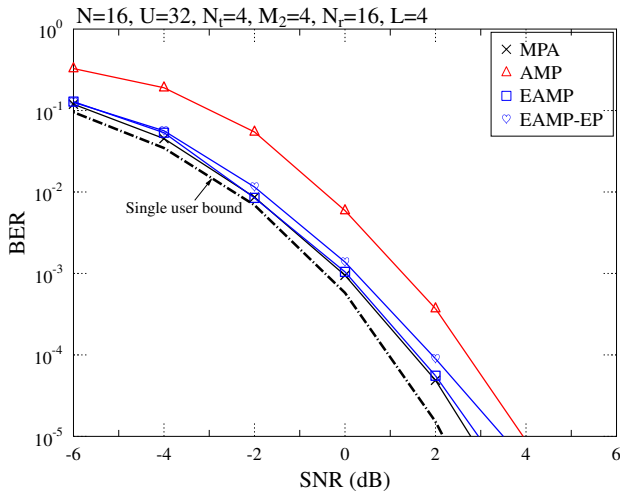
Fig. 10. The uncoded BER performance of the $N = 16$, $U = 32$ SM-SCDMA system with $N_t = 4$, $N_r = 16$ and $M_2 = 4$, when communicating over $L = 4$ frequency-selective Rayleigh fading channels, where the MPA, AMP, EAMP or EAMP-EP ($P_{th} = 0.99$) detector is employed. The throughput is 8 bpcu.

Fig. 11. The half-rate LDPC-coded BER performance of the $N = 16$, $U = 32$ SM-SCDMA system with $N_t = 4$, $N_r = 16$ and $M_2 = 4$, when communicating over $L = 4$ frequency-selective Rayleigh fading channels, where the MPA, AMP, EAMP or EAMP-EP ($P_{th} = 0.99$) detector is employed. The throughput is 4 bpcu.

as those in Figs. 6 and 7, respectively, is portrayed. The DCMC capacity per user per subcarrier shown in Fig. 5 is also included in Figs. 8 and 9 under the assumption of a half-rate code. It can be observed from Fig. 8 that the error floor has been literally eliminated with the aid of a half-rate LDPC code and the EAMP-EP detector shows a similar BER performance to that of the EAMP detector. Additionally, EAMP detection still achieves the best BER performance among the three low-complexity SM-SCDMA detectors and has only 0.7 dB performance loss at the BER of 10^{-5}, compared to the MPA detector of [16], as shown in Fig. 8.

Furthermore, when $N_r = 16$ RAs are employed, the MPA, EAMP and EAMP-EP ($P_{th} = 0.99$) detection algorithms show very similar BER performance. By contrast, when the AMP algorithm is applied without exploiting the unique properties of SM, over 2 dB performance degradation at the BER of can be observed from Fig. 9, compared to the EAMP-EP detectors.

The uncoded and coded BER performance of the MPA, AMP, EAMP or EAMP-EP detectors is shown in Figs. 10 and 11, respectively, at a normalized user load of 200%, when employing $N = 16$ subcarriers for supporting $U = 32$ users. It can be observed from Fig. 10 that both the MPA and the proposed detection algorithms achieve a similar BER performance to those of the SM-SCDMA system operating at a 150% normalized user load, as demonstrated in Fig. 7, while using $N = 16$ subcarriers. This is consistent with the results of [16], which demonstrates that the SM-SCDMA system is capable of supporting high normalized user loads of up to 200% without significant performance erosion.

Furthermore, the influence of different P_{th} values on the EAMP detector is investigated in Fig. 12, where the SM-SCDMA system associated with $N_t = 4$, $N_r = 8$, employs $N = 16$ subcarriers to support $U = 24$ users. More specifically, as shown in Fig. 12, a higher P_{th} gives a more precise approximation of the QAM symbol, hence resulting in
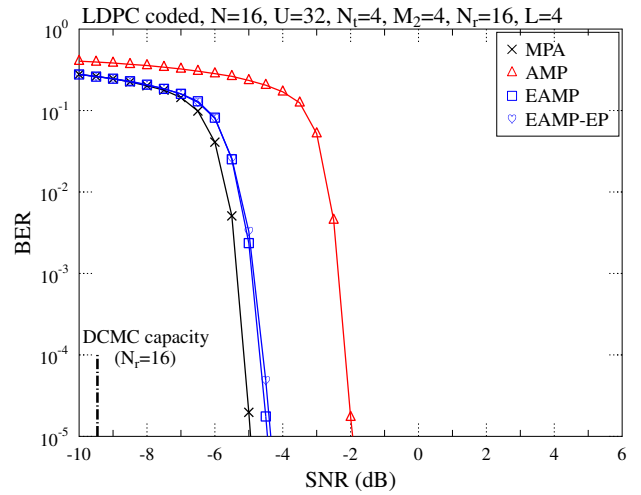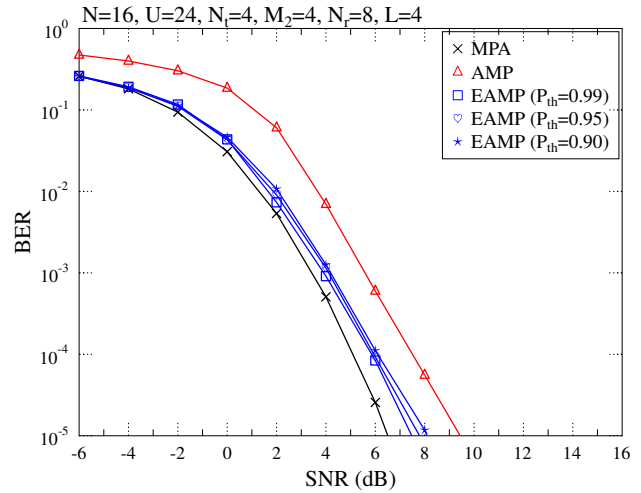
Fig. 12. The uncoded BER performance of the $N = 16$, $U = 24$ SM-SCDMA system with $N_t = 4$, $N_r = 8$ and $M_2 = 4$, when communicating over $L = 4$ frequency-selective Rayleigh fading channels, where the MPA, AMP, or EAMP detector is employed when using different P_{th} values. The throughput is 6 bpcu.

a superior BER performance. However, this is achieved at the cost of higher complexity, since more iterations are required for achieving the desired P_{th}. Since the influence of different P_{th} values on the EAPM-EP detector shows very similar BER trends to Fig. 12, the related simulation results are omitted for the sake of simplicity.

The impact of M_2 and N_t on the BER performance of our SM-SCDMA system employing the MPA or EAMP detectors is shown in Figs. 13 and 14, respectively, where $N = 16$ subcarriers are used for supporting $U = 24$ users in the SM-SCDMA system and $N_r = 8$ or 16 RAs are equipped at the BS. For explicitly demonstrating the results, the best-performed detector proposed in this paper and the benchmark
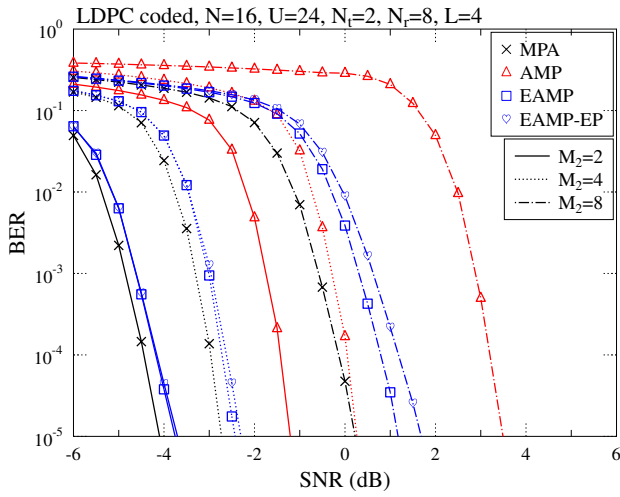
Fig. 13. The half-rate LDPC-coded BER performance of the $N = 16$, $U = 24$ SM-SCDMA system with $M_2 = 2$, $N_r = 8$ and $N_t = 2, 4$ and 8, when communicating over $L = 4$ frequency-selective Rayleigh fading channels, where the MPA, AMP, EAMP or EAMP-EP ($P_{th} = 0.99$) detector is employed.
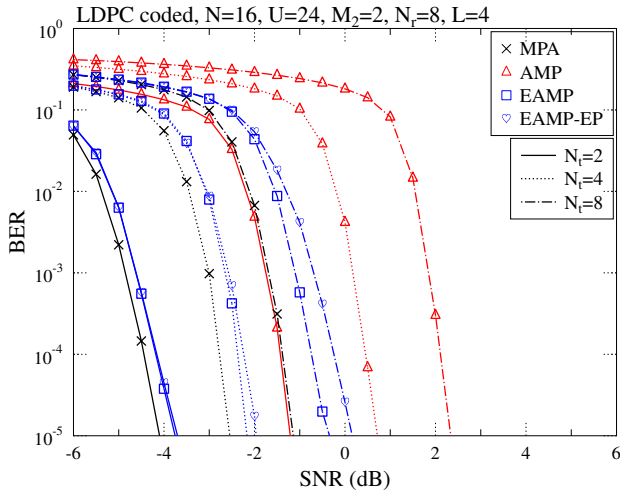
Fig. 14. The half-rate LDPC-coded BER performance of the $N = 16$, $U = 24$ SM-SCDMA system with $N_t = 2$, $N_r = 8$ and $M_2 = 2, 4$ and 8, when communicating over $L = 4$ frequency-selective Rayleigh fading channels, where the MPA, AMP, EAMP or EAMP-EP ($P_{th} = 0.99$) detector is employed.

MPA detector of [16] are included, since the influence of N_t and M_2 on the BER performance of our SM-SCDMA system using different detectors is rather similar. It can be observed from Figs. 13 and 14 that the increase of either N_t or M_2 will result in BER degradation, but a higher data rate will be attained. Additionally, increase of N_t from 4 to 8 shows more significant performance degradation than that of increasing M_2 from 4 to 8, which indicates a design trade-off between the throughput of the SSK and QAM modulation.

Finally, Fig. 15 compares the convergence behavior of the different detectors considered in this paper at different SNRs, where the BER vs. the number of iterations is portrayed for the SM-SCDMA systems employing the MPA, AMP, EAMP
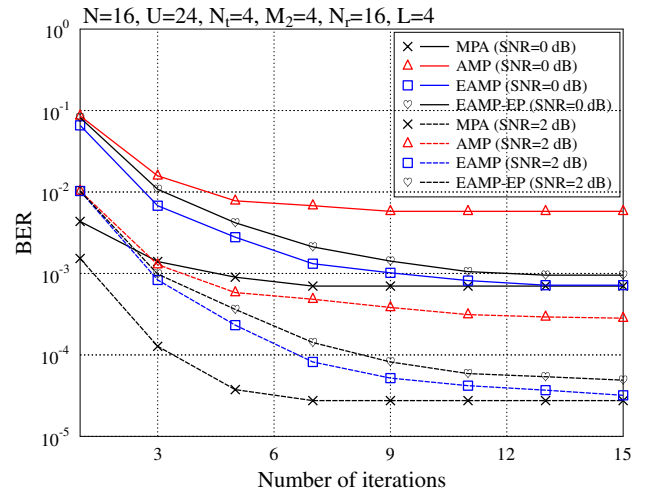
Fig. 15. The uncoded BER performance vs. the number of iterations used for the MPA, AMP, EAMP or EAMP-EP detector. The same parameters as those in Fig. 7 are employed.

or EAMP-EP detectors. The system parameters employed in Fig. 15 are the same as those in Fig. 7. It can be observed that among the four detectors, the best-performing MPA detector requires less than $I = 9$ iterations to converge, while the EAMP and EAMP-EP detectors require about 15 iterations, since IC is performed every 5 iterations for further enhancing the detection performance.

C. Complexity

In this section, the complexity of the MPA detector of [16], as well as that of the proposed AMP, EAMP and EAMP-EP detectors in terms of the average number of floating point operations (FLOPs) per iteration is analysed. More specifically, assume that

1) the multiplication of two real numbers requires a single FLOP;
2) the multiplication of a single complex number and a single real number requires 2 FLOPs;
3) the multiplication of a pair of complex numbers (excluding the conjugate multiplication) requires 6 FLOPs;
4) the multiplication of a complex number and its conjugate requires 3 FLOPs.

Also, the calculation of $\exp(\cdot)$ is assumed to be carried by a look-up table [37].

1) MPA detection: The detection complexity of the M-PA detector [16] is dominated by the upward information transmission given in (9) via the factor graph, which gives a complexity order of $\mathcal{O}[(N_t M_2)^{d_c-1} N_r U]$. The complexity per iteration of the MPA detector in terms of FLOPs was given in [41] as

$$C_{\text{MPA}} = N N_r d_u [(7 d_u - 1)(N_t M_2)^{d_u} + (d_c - 1) N_t M_2].$$
(45)

2) AMP detection: In contrast to the complexity order of the MPA detector, which increases exponentially with d_c, the AMP detector approximates the information to be transmitted

by each VN by a Gaussian distribution, ultimately resulting in linear increase with d_c, as seen in (18a). Hence, the complexity order of the EAMP detector is $\mathcal{O}[N_t M_2 (d_c - 1) N_r U]$.

More specifically, the AMP detection employs (19), (20) and (22) to (26) to complete a single iteration and each iteration requires an identical number of FLOPs. Hence, the average complexity per iteration of the AMP detector is expressed as

$$C_{\text{AMP}} = \underbrace{4UN_tM_2N_rd_c}_{(25)} + \underbrace{7UN_tM_2N_rd_c}_{(26)} + \underbrace{8NN_rN_td_u}_{(19)}$$
$$+ \underbrace{5NN_rN_td_u}_{(20)} + \underbrace{5UN_tN_rd_c}_{(23)} + \underbrace{8UN_tN_rd_c}_{(24)}$$
$$+ \underbrace{11UN_tM_2N_rd_c}_{(22)}$$
$$= (22M_2 + 16)UN_tN_rd_c. \qquad (46)$$

3) EAMP detection: The EAMP detector operates on the basis of the combinational symbol set $\bar{\mathcal{M}}$ having a size of $M_2 + 1$. If IC is not considered, the complexity order of the EAMP detector is similar to that of the AMP detector, except for the new size of the symbol set $M_2 + 1$, which can be expressed as $\mathcal{O}[N_t(M_2 + 1)(d_c - 1)N_r U]$.

Additionally, since IC is employed after a certain number of iterations, the number of edges that are used for performing (19) to (32) may be different in different iterations. Defining the number of CNs shared by the VN tu in the i-th iteration as $d_{c,tu}^{(i)}$, and the number of VNs shared by the CN rn in the i-th iteration as $d_{u,rn}^{(i)}$, then the average complexity per iteration of the EAMP detector is expressed in (47), where $C_{\text{IC-EAMP}} = \frac{11M_2 + 21}{I} \sum_{i=1}^{I/\varrho} \sum_{u=1}^{U} \sum_{t=1}^{N_t} d_{c,tu}^{(\varrho i)}$ is the average number of FLOPs per iteration required to perform IC as part of the EAMP detector.

4) EAMP-EP detection: By employing the EP algorithm to approximate the symbol belief, the computational complexity of upward information propagation is further reduced, resulting in a complexity order of $\mathcal{O}[N_t(d_c - 1)N_r U]$.

For quantifying the FLOPs required for each iterations, the EAMP-EP detection calculates the symbol belief using (37) and (38), which requires $17 \sum_{u=1}^{U} \sum_{t=1}^{N_t} d_{c,tu}^{(i)}$ FLOPs in the i-th iteration. Overall, the average complexity per iteration of the EAMP detection is expressed in (48), where $C_{\text{IC-EAMP-EP}} = \frac{22M_2 + 32}{I} \sum_{i=1}^{I/\varrho} \sum_{u=1}^{U} \sum_{t=1}^{N_t} d_{c,tu}^{(\varrho i)}$ is the average number of FLOPs per iteration required for performing IC during EAMP-EP detection.

Fig. 16 compares the overall detection complexity in terms of FLOPs for the SM-SCDMA system supporting $U = 24$ users by $N = 16$ subcarriers, when employing the MPA [16], AMP, EAMP and EAMP-EP detectors, where $M_2 = 4$, $N_t = 4$ and $N_r = 16$. As discussed in Section IV-B, $I = 9$ iterations are employed for the MPA detection, whereas the three proposed AMP-based detectors use $I = 15$ iterations. It can be observed that although the MPA detector of [16] achieves the best BER performance, as characterized in Section IV-B, this is achieved at the cost of the highest complexity. By contrast, all the three AMP-based detectors impose less than 1% of the complexity required by the MPA detector
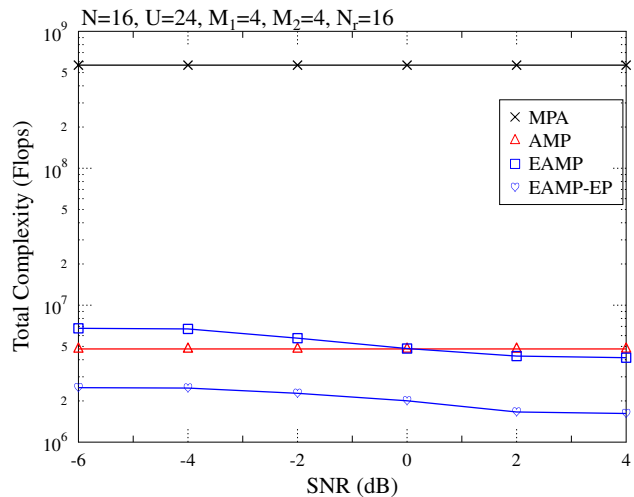
Fig. 16. The total detection complexity in terms of the number of FLOPs of the SM-SCDMA system supporting $U = 24$ users by $N = 16$ subcarriers when employing the MPA [16], AMP, EAMP and EAMP-EP detection for communication over the uncorrelated Rayleigh fading channel, where $M_2 = 4$, $N_t = 4$ and $N_r = 16$. The throughput is 6 bpcu.

to complete the iterative detection process. It can also be observed that the complexity of the MPA and AMP detectors is independent of the SNR, whereas the EAMP and EAMP-EP detectors require a lower number of FLOPs in the high SNR regions. This is because IC is adopted by both of these detectors, and when the SNR becomes high, a reduced-size factor graph is formed.

Additionally, as shown in Fig. 16, the number of FLOPs employed by the EAMP detector is similar to that of the AMP detector, even though a significant performance improvement has been demonstrated for EAMP in Section IV-B. This trend is the outcome of two different phenomena. On the one hand, the integrated symbol set $\bar{\mathcal{M}}_2$ introduced an additional symbol option and the IC operation requires extra FLOPs. These two operations result in a complexity increase. On the other hand, the IC also results in a reduced number of user signals to be detected at later iterations, hence resulting in a complexity reduction.

V. CONCLUSIONS

Three low-complexity SM-SCDMA detectors have been conceived. First, the existing AMP detector was characterized, which suffers from significant BER performance loss, compared to the state-of-the-art MPA detector. Hence, the EAMP detector was proposed, which mitigates the BER degradation by exploiting the unique properties of SM and employs an IC technique. Finally, the classic EP technique was embedded into the EAMP detector, resulting in a novel EAMP-EP detector having a further reduced detection complexity at the cost of a slightly degraded BER performance. Our results demonstrated that the proposed EAMP and EAMP-EP detectors impose on average less than 1% of the MPA detector's complexity upon completing a single iteration, at the cost of less than 1dB performance degradation at a BER of 10^{-5}, compared to that of the state-of-the-art MPA detector.

$$C_{\text{EAMP}} = \frac{1}{I} \sum_{i=1}^{I} \left[\underbrace{4(M_2+1) \sum_{u=1}^{U} \sum_{t=1}^{N_t} d_{c,tu}^{(i)}}_{(30)} + \underbrace{7(M_2+1) \sum_{u=1}^{U} \sum_{t=1}^{N_t} d_{c,tu}^{(i)}}_{(31)} + \underbrace{13 \sum_{n=1}^{N} \sum_{r=1}^{N_r} d_{u,rn}^{(i)} + 13 \sum_{u=1}^{U} \sum_{t=1}^{N_t} d_{c,tu}^{(i)}}_{(19),(20),(23),(24)} \right.$$

$$\left. + \underbrace{11(M_2+1) \sum_{u=1}^{U} \sum_{t=1}^{N_t} d_{c,tu}^{(i)}}_{(32)} \right] + \underbrace{\frac{11M_2+21}{I} \sum_{i=1}^{I/\varrho} \sum_{u=1}^{U} \sum_{t=1}^{N_t} d_{c,tu}^{(\varrho i)}}_{C_{\text{IC-EAMP}}}$$

$$= \frac{22M_2+48}{I} \sum_{i=1}^{I} \sum_{u=1}^{U} \sum_{t=1}^{N_t} d_{c,tu}^{(i)} + \frac{11M_2+21}{I} \sum_{i=1}^{I/\varrho} \sum_{u=1}^{U} \sum_{t=1}^{N_t} d_{c,tu}^{(\varrho i)}, \tag{47}$$

$$C_{\text{EAMP-EP}} = \frac{1}{I} \sum_{i=1}^{I} [\underbrace{17 \sum_{u=1}^{U} \sum_{t=1}^{N_t} d_{c,tu}^{(i)}}_{(37),(38)} + \underbrace{13 \sum_{n=1}^{N} \sum_{r=1}^{N_r} d_{u,rn}^{(i)}}_{(19),(20)}] + \underbrace{\frac{22M_2+32}{I} \sum_{i=1}^{I/\varrho} \sum_{u=1}^{U} \sum_{t=1}^{N_t} d_{c,tu}^{(\varrho i)}}_{C_{\text{IC-EAMP-EP}}}$$

$$= \frac{30}{I} \sum_{i=1}^{I} \sum_{u=1}^{U} \sum_{t=1}^{N_t} d_{c,tu}^{(i)} + \frac{22M_2+32}{I} \sum_{i=1}^{I/\varrho} \sum_{u=1}^{U} \sum_{t=1}^{N_t} d_{c,tu}^{(\varrho i)}, \tag{48}$$

REFERENCES

[1] R. Y. Mesleh, H. Haas, S. Sinanovic, C. W. Ahn, and S. Yun, "Spatial modulation," *IEEE Transactions on Vehicular Technology*, vol. 57, no. 4, pp. 2228–2241, 2008.

[2] M. Di Renzo, H. Haas, A. Ghrayeb, S. Sugiura, and L. Hanzo, "Spatial modulation for generalized MIMO: Challenges, opportunities, and implementation," *Proceedings of the IEEE*, vol. 102, no. 1, pp. 56–103, 2014.

[3] P. Yang, M. Di Renzo, Y. Xiao, S. Li, and L. Hanzo, "Design guidelines for spatial modulation," *IEEE Communications Surveys & Tutorials*, vol. 17, no. 1, pp. 6–26, 2015.

[4] J. Jeganathan, A. Ghrayeb, L. Szczecinski, and A. Ceron, "Space shift keying modulation for MIMO channels," *IEEE Transactions on Wireless Communications*, vol. 8, no. 7, pp. 3692–3703, 2009.

[5] R. Mesleh, S. S. Ikki, and H. M. Aggoune, "Quadrature spatial modulation," *IEEE Transactions on Vehicular Technology*, vol. 64, no. 6, pp. 2738–2742, 2014.

[6] J. Wang, S. Jia, and J. Song, "Generalised spatial modulation system with multiple active transmit antennas and low complexity detection scheme," *IEEE Transactions on Wireless Communications*, vol. 11, no. 4, pp. 1605–1615, 2012.

[7] R. Rajashekar, K. Hari, and L. Hanzo, "Transmit antenna subset selection in spatial modulation relying on a realistic error-infested feedback channel," *IEEE Access*, vol. 6, pp. 5879–5890, 2017.

[8] C. Wang, P. Cheng, Z. Chen, J. A. Zhang, Y. Xiao, and L. Gui, "Near-ML low-complexity detection for generalized spatial modulation," *IEEE Communications Letters*, vol. 20, no. 3, pp. 618–621, 2016.

[9] L. Xiao, P. Yang, Y. Xiao, S. Fan, M. Di Renzo, W. Xiang, and S. Li, "Efficient compressive sensing detectors for generalized spatial modulation systems," *IEEE Transactions on Vehicular Technology*, vol. 66, no. 2, pp. 1284–1298, 2016.

[10] L. Xiao, Y. Xiao, C. Xu, X. Lei, P. Yang, S. Li, and L. Hanzo, "Compressed-sensing assisted spatial multiplexing aided spatial modulation," *IEEE Transactions on Wireless Communications*, vol. 17, no. 2, pp. 794–807, 2017.

[11] Q. Tang, Y. Xiao, P. Yang, Q. Yu, and S. Li, "A new low-complexity near-ML detection algorithm for spatial modulation," *IEEE Wireless Communications Letters*, vol. 2, no. 1, pp. 90–93, 2012.

[12] L.-L. Yang, "Signal detection in antenna-hopping space-division multiple-access systems with space-shift keying modulation," *IEEE Transactions on Signal Processing*, vol. 60, no. 1, pp. 351–366, 2012.

[13] P. Pan and L.-L. Yang, "Spatially modulated code-division multiple-access for high-connectivity multiple access," *IEEE Transactions on Wireless Communications*, vol. 18, no. 8, pp. 4031–4046, 2019.

[14] Y. Liu, L. Yang, and L. Hanzo, "Spatial modulation aided sparse code-division multiple access," *IEEE Transactions on Wireless Communications*, vol. 17, no. 3, pp. 1474–1487, March 2018.

[15] Z. Wang, J. Cao *et al.*, "NOMA-based spatial modulation," *IEEE Access*, vol. 5, pp. 3790–3800, 2017.

[16] Y. Liu, L.-L. Yang, P. Xiao, H. Haas, and L. Hanzo, "Spatial modulated multicarrier sparse code-division multiple access," *IEEE Transactions on Wireless Communications*, vol. 19, no. 1, pp. 610–623, 2020.

[17] X. Chen, M. Wen, and S. Dang, "On the performance of cooperative OFDM-NOMA system with index modulation," *IEEE Wireless Communications Letters*, vol. 9, no. 9, pp. 1346–1350, 2020.

[18] K. Lai, J. Lei, L. Wen, and G. Chen, "Codeword position index modulation design for sparse code multiple access system," *IEEE Transactions on Vehicular Technology*, vol. 69, no. 11, pp. 13 273–13 288, 2020.

[19] Y. Liu, L.-L. Yang, and L. Hanzo, "Sparse space-time-frequency-domain spreading for large-scale non-orthogonal multiple access," *IEEE Transactions on Vehicular Technology*, vol. 69, no. 10, pp. 12 327–12 332, 2020.

[20] F. Tekçe, U. E. Ayten, and L. Durak-Ata, "SCMA system design with index modulation via codebook assignment," *IEEE Transactions on Vehicular Technology*, vol. 70, no. 2, pp. 1699–1708, 2021.

[21] R. Hoshyar, F. P. Wathan, and R. Tafazolli, "Novel low-density signature for synchronous CDMA systems over AWGN channel," *IEEE Transactions on Signal Processing*, vol. 56, no. 4, pp. 1616–1626, 2008.

[22] C. Zhong, X. Hu, X. Chen, D. W. K. Ng, and Z. Zhang, "Spatial modulation assisted multi-antenna non-orthogonal multiple access," *IEEE Wireless Communications*, vol. 25, no. 2, pp. 61–67, 2018.

[23] Z. Na, Y. Liu, J. Shi, C. Liu, and Z. Gao, "UAV-supported clustered NOMA for 6G-enabled Internet of things: Trajectory planning and resource allocation," *IEEE Internet of Things Journal*, 2020.

[24] M. Mohammadkarimi, M. A. Raza, and O. A. Dobre, "Signature-based nonorthogonal massive multiple access for future wireless networks: Uplink massive connectivity for machine-type communications," *IEEE Vehicular Technology Magazine*, vol. 13, no. 4, pp. 40–50, 2018.

[25] S. Han, X. Xu, S. Fang, Y. Sun, Y. Cao, X. Tao, and P. Zhang, "Energy efficient secure computation offloading in NOMA-based mMTC networks for IoT," *IEEE Internet of Things Journal*, vol. 6, no. 3, pp. 5674–5690, 2019.

[26] Y. Liu, L. L. Yang, and L. Hanzo, "Joint user-activity and data detection for grant-free spatial-modulated multi-carrier non-orthogonal multiple access," *IEEE Transactions on Vehicular Technology*, vol. 69, no. 10, pp. 11 673–11 684, 2020.

[27] I. Al-Nahhal, O. A. Dobre, E. Basar, and S. Ikki, "Low-cost uplink sparse code multiple access for spatial modulation," *IEEE Transactions on Vehicular Technology*, vol. 68, no. 9, pp. 9313–9317, 2019.

[28] I. Al-Nahhal, O. A. Dobre, and S. Ikki, "On the complexity reduction of uplink sparse code multiple access for spatial modulation," *IEEE Transactions on Communications*, vol. 68, no. 11, pp. 6962–6974, 2020.

[29] L. Liu, C. Yuen, Y. L. Guan, Y. Li, and C. Huang, "Gaussian message passing for overloaded massive MIMO-NOMA," *IEEE Transactions on Wireless Communications*, vol. 18, no. 1, pp. 210–226, 2018.

[30] P. Wang, L. Liu, S. Zhou, G. Peng, S. Yin, and S. Wei, "Near-optimal MIMO-SCMA uplink detection with low-complexity expectation propagation," *IEEE Transactions on Wireless Communications*, vol. 19, no. 2, pp. 1025–1037, 2020.

[31] J. Dai, K. Niu, and J. Lin, "Iterative Gaussian-approximated message passing receiver for MIMO-SCMA system," *IEEE Journal of Selected Topics in Signal Processing*, vol. 13, no. 3, pp. 753–765, 2019.

[32] Z. Gao, L. Dai, Z. Wang, S. Chen, and L. Hanzo, "Compressive-sensing-based multiuser detector for the large-scale SM-MIMO uplink," *IEEE Transactions on Vehicular Technology*, vol. 65, no. 10, pp. 8725–8730, 2015.

[33] A. Garcia-Rodriguez and C. Masouros, "Low-complexity compressive sensing detection for spatial modulation in large-scale multiple access channels," *IEEE Transactions on Communications*, vol. 63, no. 7, pp. 2565–2579, 2015.

[34] X. Meng, S. Wu, L. Kuang, D. Huang, and J. Lu, "Multi-user detection for spatial modulation via structured approximate message passing," *IEEE Communications Letters*, vol. 20, no. 8, pp. 1527–1530, 2016.

[35] A. Graham, "Kronecker products and matrix calculus: With applications." *JOHN WILEY & SONS, INC., 605 THIRD AVE., NEW YORK, NY 10158, 1982, 130*, 1982.

[36] L.-L. Yang, *Multicarrier Communications*. Chichester, United Kingdom: John Wiley, 2009.

[37] S. Wu, L. Kuang, Z. Ni, J. Lu, D. Huang, and Q. Guo, "Low-complexity iterative detection for large-scale multiuser MIMO-OFDM systems using approximate message passing," *IEEE Journal of Selected Topics in Signal Processing*, vol. 8, no. 5, pp. 902–915, 2014.

[38] A. Gelman, J. B. Carlin, H. S. Stern, D. B. Dunson, A. Vehtari, and D. B. Rubin, *Bayesian data analysis*. CRC press, 2013.

[39] D. Koller and N. Friedman, *Probabilistic graphical models: principles and techniques*. MIT press, 2009.

[40] S. X. Ng and L. Hanzo, "On the MIMO channel capacity of multidimensional signal sets," *IEEE Transactions on Vehicular Technology*, vol. 55, no. 2, pp. 528–536, 2006.

[41] Z. Tang, J. Wang, J. Wang, and J. Song, "A low-complexity detection algorithm for uplink NOMA system based on Gaussian approximation," in *2017 IEEE Wireless Communications and Networking Conference (WCNC)*. IEEE, 2017, pp. 1–6.